



LUND UNIVERSITY

Performance of the AGATA Gamma-ray Spectrometer in the PreSPEC Set-up at GSI

Lalovic, Natasa; Louchart, C.; Michelagnoli, C.; Perez-Vidal, R.M.; Ralet, D.; Gerl, J.; Rudolph, Dirk; Arici, T.; Bazzacco, D.; Clement, E.; Gadea, A.; Kojouharov, I.; Korichi, A.; Labiche, M.; Ljungvall, J.; Lopez-Martens, A.; Nyberg, J.; Pietralla, N.; Pietri, S.; Stezowski, O.; Collaboration, the AGATA; Collaboration, the PreSPEC

Published in:

Nuclear Instruments & Methods in Physics Research. Section A: Accelerators, Spectrometers, Detectors, and Associated Equipment

DOI:

[10.1016/j.nima.2015.10.032](https://doi.org/10.1016/j.nima.2015.10.032)

2016

[Link to publication](#)

Citation for published version (APA):

Lalovic, N., Louchart, C., Michelagnoli, C., Perez-Vidal, R. M., Ralet, D., Gerl, J., Rudolph, D., Arici, T., Bazzacco, D., Clement, E., Gadea, A., Kojouharov, I., Korichi, A., Labiche, M., Ljungvall, J., Lopez-Martens, A., Nyberg, J., Pietralla, N., Pietri, S., ... Collaboration, T. PPEC. (2016). Performance of the AGATA Gamma-ray Spectrometer in the PreSPEC Set-up at GSI. *Nuclear Instruments & Methods in Physics Research. Section A: Accelerators, Spectrometers, Detectors, and Associated Equipment*, 806, 258-266.
<https://doi.org/10.1016/j.nima.2015.10.032>

Total number of authors:

22

General rights

Unless other specific re-use rights are stated the following general rights apply:

Copyright and moral rights for the publications made accessible in the public portal are retained by the authors and/or other copyright owners and it is a condition of accessing publications that users recognise and abide by the legal requirements associated with these rights.

- Users may download and print one copy of any publication from the public portal for the purpose of private study or research.
- You may not further distribute the material or use it for any profit-making activity or commercial gain
- You may freely distribute the URL identifying the publication in the public portal

Read more about Creative commons licenses: <https://creativecommons.org/licenses/>

Take down policy

If you believe that this document breaches copyright please contact us providing details, and we will remove access to the work immediately and investigate your claim.

LUND UNIVERSITY

PO Box 117
221 00 Lund
+46 46-222 00 00

Performance of the AGATA γ -ray Spectrometer in the PreSPEC Set-up at GSI

N. Lalović^{a,b}, C. Louchart^c, C. Michelagnoli^d, R. M. Perez-Vidal^e, D. Ralet^{b,c},
J. Gerl^b, D. Rudolph^a, T. Arici^{f,b}, D. Bazzacco^g, E. Clément^d, A. Gadea^e,
I. Kojouharov^b, A. Korichi^h, M. Labicheⁱ, J. Ljungvall^h, A. Lopez-Martens^h,
J. Nyberg^j, N. Pietralla^c, S. Pietri^b, O. Stezowski^k, and the PreSPEC and
AGATA Collaborations

^a*Department of Physics, Lund University, SE-22100 Lund, Sweden*

^b*GSI Helmholtzzentrum für Schwerionenforschung GmbH, D-64291 Darmstadt, Germany*

^c*Institut für Kernphysik, Technische Universität Darmstadt, D-64289 Darmstadt, Germany*

^d*GANIL, CEA/DSM-CNRS/IN2P3, BP 55027, F-14076 Caen, France*

^e*Instituto de Física Corpuscular, CSIC-Universitat de Valencia, E-46920 Valencia, Spain*

^f*Justus-Liebig-Universität Giessen, D-35392 Giessen, Germany*

^g*INFN Sezione di Padova and Dipartimento di Fisica, Università di Padova, IT-35131
Padova, Italy*

^h*CSNSM, F-91405 Orsay Campus, France*

ⁱ*STFC Daresbury Laboratory, Daresbury, WA4 4AD Warrington, UK*

^j*Department of Physics and Astronomy, Uppsala University, SE-75120 Uppsala, Sweden*

^k*Université de Lyon, CNRS-IN2P3, Institut de Physique Nucléaire de Lyon, F-69622
Villeurbanne, France*

Abstract

1 In contemporary nuclear physics, the European Advanced GAMMA Tracking
2 Array (AGATA) represents a crucial detection system for cutting-edge nuclear
3 structure studies. AGATA consists of highly segmented high-purity germanium
4 crystals and uses the pulse-shape analysis technique to determine both the po-
5 sition and the energy of the γ -ray interaction points in the crystals. It is the
6 tracking algorithms that deploy this information and enable insight into the
7 sequence of interactions, providing information on the full or partial absorption
8 of the γ ray. A series of dedicated performance measurements for an AGATA
9 set-up comprising 21 crystals is described. This set-up was used within the re-
10 cent PreSPEC-AGATA experimental campaign at the GSI Helmholtzzentrum
11 für Schwerionenforschung. Using the radioactive sources ^{56}Co , ^{60}Co and ^{152}Eu ,
12 absolute and normalized efficiencies and the peak-to-total of the array were mea-
13 sured. These quantities are discussed using different data analysis procedures.

Email address: Natasa.Lalovic@nuclear.lu.se (N. Lalović)

14 The quality of the pulse-shape analysis and the tracking algorithm are evaluated.
15 The agreement between the experimental data and the Geant4 simulations is
16 also investigated.

Keywords: AGATA, gamma-ray spectroscopy, gamma-ray tracking, nuclear
structure, pulse shape analysis, HPGe detectors

17 **1. Introduction**

18 Numerous exciting nuclear-structure phenomena can be probed by in-beam
19 γ -ray spectroscopy experiments. Innovative approaches in design of dedicated
20 detection systems during the past decades led to significant advances in position
21 sensitivity, photopeak efficiency and peak-to-total ratio (P/T) in γ -ray spec-
22 troscopy. Moreover, the most recent γ -ray spectrometers, such as AGATA [1]
23 and GRETA [2], brought about the new concept of high-resolution germanium
24 tracking arrays. This paper starts out with a retrospective overview of large
25 γ -ray arrays (Sec. 2) in order to introduce the developments and requirements
26 of the new tracking arrays.

27 Here, the focus is the performance of AGATA in the framework of the re-
28 cent PreSPEC-AGATA campaign at the GSI Helmholtzzentrum für Schwerio-
29 nenforschung, Darmstadt, Germany [3, 4]. Incoming particle identification is
30 done event by event by Fragment Separator (FRS) detector systems [5]. De-
31 tails of the AGATA subarray configured for the PreSPEC-AGATA campaign
32 are presented in Sec. 3.

33 Using Monte Carlo simulations based on the Geant4 toolkit [6], extensive
34 characterization studies of AGATA were performed [7, 8]. Nevertheless, it is im-
35 portant for the feasibility and the success of the present and future experiments
36 to check experimentally the validity and reliability of this simulation tool, as
37 well as the calculated performance figures. Therefore, a dedicated source mea-
38 surement was performed and is described in detail in Sec. 4. Furthermore, the
39 quantities such as photopeak efficiency, normalized efficiency as a function of
40 the γ -ray energy and P/T were investigated following the procedure outlined in

41 Sec. 5. The results of the analysis performed on the data alongside their inter-
 42 pretation and effect on other measurements are presented in Sec. 6. Moreover,
 43 these results were confronted to the output of the Geant4 simulation and their
 44 agreement is presented in Sec. 7.

45 Finally, the paper concludes with a short summary and an outlook for further
 46 investigations of performance of AGATA at GSI.

47 **2. Concept of γ -ray Detection with AGATA**

48 The strength of AGATA is the ability to obtain positions and deposited ener-
 49 gies of individual γ -ray interactions. Applying γ -ray tracking makes it possible
 50 to determine the sequence of the interactions.

51 The sophisticated design of AGATA came about only after a series of ad-
 52 vancements of large γ -ray detector arrays [9, 10]. At a very early stage of HPGe
 53 detectors' development, studies of nuclear structure could benefit from larger
 54 individual detectors, in comparison with Li-drifted Ge detectors. Further im-
 55 provements focused on the increase of both the number of detectors and the solid
 56 angle covered by an array. This led to an enhancement of detection properties,
 57 mainly efficiency and energy resolution, and to some extent P/T . Additionally,
 58 a technique of background reduction was developed by means of Compton sup-
 59 pression. These efforts gave rise to the first arrays of HPGe detectors actively
 60 shielded by scintillating materials, which provided a substantial improvement
 61 of P/T .

62 Once a γ ray interacts with the detector medium, the energy recorded by
 63 those conventional arrays is the signal of any individual Ge-detector crystal.
 64 Typically, the absolute photopeak efficiency here depends on the intrinsic effi-
 65 ciency of the detector and its distance to the source. The P/T is determined
 66 by the intrinsic P/T of the individual detector elements, i.e. Ge detector plus
 67 surrounding Compton-suppression shield, and its geometry.

68 The next generation of Ge arrays relied on the novel idea of producing com-
 69 posite detectors, in particular the clover [11] and the cluster [12, 13] detectors.

Such detectors overcame the size limitation of the germanium crystals, while maintaining high granularity. This is important for the detection of long cascades of coincident γ rays. Arrays based on composite detectors increased efficiency over a large energy range and showed excellent P/T performance, thanks to the 'add back' concept [14], that uses signals from neighbouring Ge-detector crystals. Not only are the events originating in individual detectors summed to generate the total energy signal, but also the fraction of energies is recorded in cases of scattering between the crystals.

However, those detectors cover relatively large solid angles. This implies an uncertainty in γ -ray detection angle and quickly leads to Doppler-broadened peaks when studying γ -ray decays of fast-moving sources [15]. Secondly, it is difficult to distinguish two (or more) γ rays interacting at the same time in the same detector. This can lead to summing effects of coincident γ -ray transitions. The fact that those two γ rays are counted as one reduces the gain in efficiency and P/T provided by the advancement of composite detectors. Therefore, in the next generation of large γ -ray arrays the granularity was increased by means of additional contact segmentation [16, 17].

The innovative concept of segmentation ensured smaller opening angles of the individual granuli, which allowed for shorter detector-to-source distance, without deteriorating energy resolution due to Doppler broadening. As a consequence, the efficiency improved significantly [8]. The first arrays had longitudinal segmentation and made the localisation of the first interaction point in a two-dimensional plane possible [16, 17]. In this generation of detector arrays it was not the opening angle of the crystal as a unity that affected the Doppler broadening, but that of an individual segment instead. The above mentioned summing effects are also significantly reduced. Finally, the P/T of such detector arrangements can be enhanced.

The most recent developments followed the line of segmentation introduced above, and the idea of γ -ray tracking was realized through the three-dimensional segmentation (longitudinal and azimuthal) of HPGe crystals of specific tapered shape. The prerequisite to tracking are the determined interaction points pro-

101 vided by the pulse-shape analysis (PSA). As a consequence, Compton-suppression
 102 shields can be excluded. This allows to fill significantly more solid angle with
 103 Ge detectors. Currently two systems based on this principle are operational,
 104 one being in the U.S.A., GRETINA [2], and one in Europe, AGATA [1, 18–20].

105 The present work provides the feedback on the application of PSA algo-
 106 rithms and helps to evaluate the reconstruction quality with respect to all three
 107 coordinates, x , y and z .

108 There are two types of algorithms dealing with the tracking of the subsequent
 109 interactions of a γ -ray in a Ge crystal. The first one, which is called back-
 110 tracking [21, 22], is based on the reconstruction of the γ -ray path by starting
 111 the tracking procedure from the final interaction point. The second one is called
 112 forward-tracking [23–25] and starts by first recognizing clusters of interaction
 113 points. In this work, the forward-tracking algorithm is used and the results of
 114 the optimization are presented in Sec. 6.

115 3. AGATA Detector Configuration at GSI

116 In preparation for the HISPEC experiment at the FAIR-NuSTAR facility
 117 [26], the PreSPEC-AGATA campaign [3, 4] was conducted at GSI in 2012 and
 118 2014. Here, secondary radioactive beams are produced by fission or fragmenta-
 119 tion of a primary stable beam delivered by GSI accelerator complex and selected
 120 by the FRS [5]. These beams are directed to a secondary target at relativistic
 121 energies of several hundred MeV/u. The in-flight emitted γ rays coming from
 122 the secondary reactions are therefore affected by a significant Doppler shift:
 123 the sources are moving with velocities of about 50 % of the speed of light. The
 124 products of secondary nuclear reactions were discriminated using the Lund York
 125 Cologne CALorimeter (LYCCA) [27].

126 The AGATA subarray, composed of 21 encapsulated detectors was placed
 127 at its nominal distance of 23.5 cm to the centre of the secondary target. Such
 128 a configuration ensured optimal energy resolution of Doppler-corrected γ -ray
 129 spectra, alongside the improved efficiency of the array compared with the earlier

130 RISING fast-beam set-up [15]. However, compared with the full AGATA array,
 131 this geometrical configuration results in only about 60 % of the crystal surfaces
 132 in contact with neighbouring ones. Thus the probability of γ rays escaping
 133 the active Ge volume is rather large, which limits the tracking performance
 134 compared to a full 4π tracking array.

135 According to the original design [1], AGATA consists of triple clusters of Ge
 136 crystals (cf. Fig. 1). Hosting AGATA at the final focal plane of the FRS required
 137 a modified arrangement. Because of the rather large beam-spot size, the most
 138 inner ring of five triple clusters needed to be replaced. Newly developed double
 139 clusters were then put in place to guarantee angular coverage at forward angles.
 140 This is due to the Lorentz boost, which has to be considered in case of γ rays
 141 emitted from nuclei moving at relativistic energies.

142 The arrangement of AGATA detectors in doubles and triples is shown in
 143 Fig. 1. The triples are enclosed by blue lines and the doubles by green lines.
 144 Dashed lines refer to missing crystals in two triple clusters, as well as one crystal
 145 from an AGATA double. Its electronics was used for the EUROBALL reference
 146 capsule (see Sec. 4).

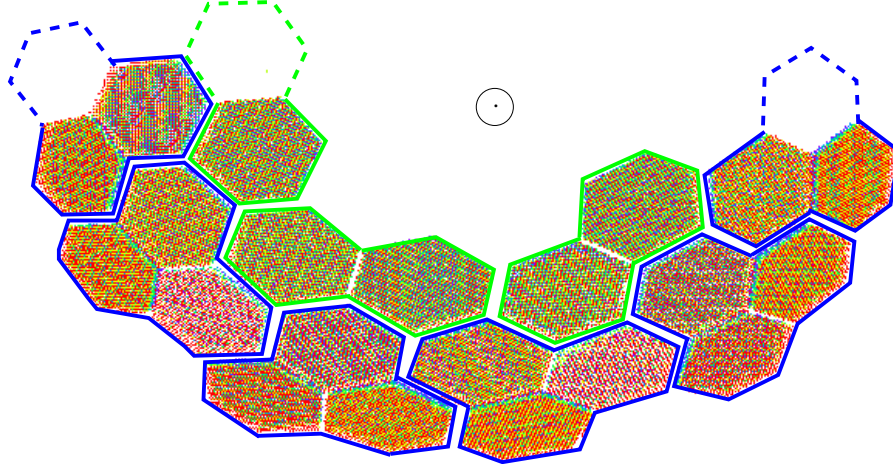


Figure 1: Configuration of AGATA at GSI during the PreSPEC-AGATA campaign. AGATA triples are enclosed by blue lines and AGATA doubles by green lines. Dashed lines indicate missing crystals. The \odot symbol marks the beam direction.

147 4. Source Measurements

148 In order to analyze the in-beam experimental data, it is necessary to de-
149 termine the response of the spectrometer by measuring efficiency and P/T .
150 As mentioned before, simulations can be an excellent way to characterize, in
151 a broad energy range, the performance figures for the campaigns employing
152 AGATA. Nevertheless, simulated figures need to be checked thoroughly and,
153 therefore, source measurements are required.

154 Early measurements at both LNL and GSI were severely hampered by fac-
155 tors such as the reduced number of encapsulated detectors present in the set-up,
156 the uncertainties about the source position, the radiation background, the data
157 acquisition dead time, to name but a few. Hence, a series of dedicated source
158 measurements focusing on the determination of the absolute efficiency was per-
159 formed within the scope of the PreSPEC-AGATA campaign at GSI in 2014.

160 The principal set-up comprised 21 36-fold segmented AGATA crystals po-
161 sitioned at the nominal target-array distance of 23.5 cm and one external non-
162 segmented and electrically cooled detector [28], based on an EUROBALL cap-
163 sule [12] as a reference (cf. Fig.2). It was intended to extract the absolute
164 quantities, such as photopeak efficiency and P/T , in the most reliable manner.
165 This was ensured by an approach, which is based on prompt coincidences of
166 cascading γ rays between the external reference detector, i.e. the EUROBALL
167 capsule, and all AGATA crystals.

168 Each of the AGATA crystals provides 38 signals: 36 for the segments and
169 two for the core, namely two gains corresponding to a 5-MeV and a 30-MeV
170 full range. The output of the respective preamplifier is digitized by means of
171 a 100-MHz 14-bit ADC. This information is then sent via optical links to pre-
172 processing cards, which perform the task of extracting the energy and time of a
173 particular detector element [1]. To access the energy and time information, the
174 Moving-Window Deconvolution (MWD) technique [29] and a leading-edge algo-
175 rithm have been used, respectively. The outputs of this stage are transmitted
176 to a computer farm performing further data processing, the overview of which

177 is given in Ref. [30]. For more details on the complete data acquisition system
178 employed in the PreSPEC-AGATA campaign, see Ref. [31].

179 For the source measurements, the electrically cooled EUROBALL capsule
180 was integrated into the system in such a way that the signal from its preamplifier
181 was sent to one of the AGATA digitizers. This ensured the same treatment of
182 all crystals used for this measurement during data-taking. However, the fact
183 that not all AGATA-tailored processing algorithms can be applied to or are
184 relevant for the EUROBALL capsule led to further differentiation between these
two detector types in the offline analysis. Data has been taken with standard

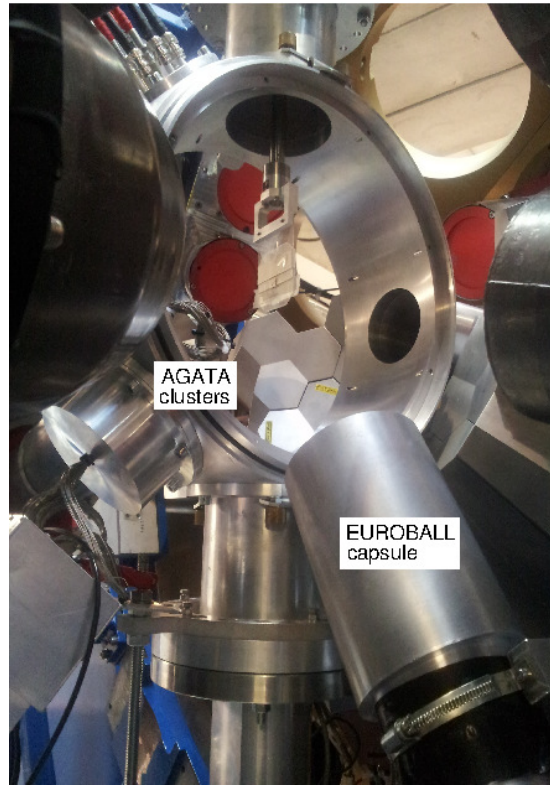


Figure 2: Part of the experimental set-up with the EUROBALL capsule, target station, and some AGATA clusters visible in the back. The EUROBALL capsule is located in the lower right corner.

185

186 γ -ray sources: ^{56}Co , ^{60}Co and ^{152}Eu . Each source was placed at the target

position in the center of the PreSPEC-AGATA scattering chamber. During the in-beam experiments, this chamber holds the secondary target, so that the γ rays emitted from the target are to be detected by the surrounding array. For the measurements described here, the side parts of the scattering chamber were dismantled, whereas the holding ring structure was left in place. This can be seen in Fig. 2. The self-triggered data acquisition was handling the data generated by event rates up to 4 - 5 kHz per crystal.

In order to make a reliable efficiency estimate of direct use for the analysis of the stopped-beam experiments, the ^{60}Co and ^{152}Eu sources were also placed in front of and behind the plastic stopper. This 1 cm thick stopper was located 15 cm downstream from the focal point of the AGATA subarray. Then, averaging measurements of these two source positions, the efficiency values are extracted for the center of the plastic stopper. This position is denoted 'close position'. However, since these measurements were performed in between two in-beam experiments, additional material was present around the scattering chamber, namely its side parts and a 2 mm thick lead shielding. This has to be taken into account when interpreting particularly the low energy region of the spectra recorded under these conditions.

5. Analysis

5.1. Fine Tuning Prior to the Analysis

The processing of the signals from individual AGATA crystals and the essential calibration aspects are detailed in Ref. [30]. The processing takes place on two levels: on the *local* level all crystals are handled separately; on the *global* level the streams of processed data from individually treated crystals are assembled on the basis of time-stamp and processed further as events. The sequence of processing stages and a schematic overview are outlined in Appendix A.

In order to derive the interaction positions a number of tests with several PSA algorithms was performed. Although different, those algorithms had no apparent effect on the results and the analysis was conducted with the standard

216 PSA algorithm, Adaptive Grid Search [33], considering single interaction in a
217 segment.

218 Since the EUROBALL capsule was integrated as if it were one of the AGATA
219 crystals, its data was processed in the same way as an AGATA crystal.

220 In this measurement events were constructed using all the data from the
221 crystals within a time window of 100 ns. Thereafter, the tracking algorithm
222 was applied on the AGATA data exclusively, which is discussed thoroughly in
223 Sec. 5.2.

224 5.2. Absolute Efficiency and Peak-to-Total

225 One of the main tasks of the data analysis was to determine the absolute effi-
226 ciency of the AGATA array, depending on data treatment and parametrization.
227 Thereby, two different approaches have been employed. The data taken with a
228 ^{60}Co source utilizes its cascade of two coincident γ rays at 1332 and 1173 keV.
229 In the first approach, the so-called *external trigger method*, the coincidences be-
230 tween AGATA crystals and the EUROBALL capsule as a reference are studied.
231 The second approach is the *sum-peak method*, focusing on AGATA crystals only
232 where no coincidences were used. In the external trigger method, a $\gamma\gamma$ angular
233 correlation correction of 0.981(5) is applied for the ^{60}Co cascade, corresponding
234 to the average angle between the AGATA crystals and the EUROBALL capsule.

235 5.2.1. External Trigger Method

236 Events which fulfilled the trigger requirement from the reference detector
237 within a 100 ns time window were selected for this approach. The energy spectra
238 representative for the whole array were created, depending on the modes in
239 which AGATA can be operated at the data-analysis stage:

- 240 • core common: takes into account individual energies registered by the
241 central contacts;
- 242 • calorimetric: total sum of energies recorded by all central contacts of all
243 AGATA crystals;

- 244 • tracked: uses the reconstructed energy, which is subject to the tracking
245 performance and thus choice of tracking parameters.
- 246 • tracked, excluding single interaction: same as the previous mode except
247 that it discards events with only a single interaction point up to the energy
248 of 800 keV.
- 249 • add-back: selectively sums single hits in an event found within a sphere
250 of 100 mm radius. The reference point for this approach was the hit with
251 maximum energy deposition.

252 The absolute efficiency at 1173 keV in all five analysis modes is extracted
253 from the ratio of the intensity in the 1173 keV peak measured by AGATA
254 crystals over the intensity of the 1332 keV peak measured by the EUROBALL
255 capsule. In this case, P/T was calculated as a ratio of the yield of the peak at
256 1173 keV and the total number of counts in the spectrum.

257 Furthermore, in case of the tracking mode of analysis, the impact of the
258 AGATA tracking algorithms on the performance was studied. This is explained
259 in more detail in Sec. 6.3.

260 5.2.2. *Sum-Peak Method*

261 In this approach, the absolute efficiency was determined using the sum-peak
262 method [34, 35]. Data collected by the reference detector was not used in this
263 case. AGATA was treated as a calorimeter, resulting in a total spectrum where
264 the energies from all central contacts have been summed up. Thus, the absolute
265 efficiency at 1173 keV was measured from the ratio of the intensity in the sum-
266 peak at 2505 keV over the intensity of the 1332 keV peak. In this case, P/T was
267 calculated as a ratio of the sum of the ^{60}Co peaks intensities and the total counts
268 in the spectra up to 1350 keV. For a reliable efficiency estimate, a correction
269 for random coincidences was performed, quantifying it from the activity of the
270 source used in the measurement. Additionally, rare cases of multiple cascades
271 have also been accounted for.

272 The use of the external trigger method was motivated in Sec. 4 as the most
 273 reliable method to extract the absolute efficiency, hence the thorough considera-
 274 tion of different analysis modes. In contrast, for the sum-peak method only the
 275 calorimetric mode of analysis was used to simply cross check the values obtained
 276 with the external trigger method.

277 *5.3. Normalized Efficiency*

278 Data taken with the ^{56}Co and ^{152}Eu sources provide the energy dependence
 279 of the efficiency in the γ -ray energy range from 120 to 3300 keV. To combine
 280 the two data sets collected with the two aforementioned sources separately, the
 281 spectrum of the former was normalized with respect to the 867-keV line of the
 282 latter, since the ^{56}Co source emits a γ ray of similar energy, namely 847 keV.
 283 For this method, calorimetric, core common and the tracked mode of analysis
 284 were used.

285 Data taken with the ^{152}Eu source alone has also been analyzed by means
 286 of the add-back routine. To normalize the yields obtained in this way, the
 287 absolute efficiency from the external trigger method was utilized (see Sec. 5.2.1).
 288 Furthermore, performance of the tracking has been tested on the data taken with
 289 the ^{152}Eu source only (see Sec. 6.3).

290 In order to obtain the normalized efficiency curve for the stopped-beam data
 291 from the PreSPEC-AGATA campaign, data collected with the ^{152}Eu source at
 292 the so-called 'close position' (see Sec. 4) has been analyzed. Thereby, the energy
 293 information from the central contact of all crystals was employed. Finally, the
 294 yields of standard γ lines recorded at two different positions were averaged and
 295 normalized to the absolute efficiency.

296 **6. Results**

297 *6.1. Absolute Efficiency and Peak-to-Total*

298 The values obtained for the absolute efficiency and P/T values at 1173 keV
 299 are shown in Table 1.

Table 1: Efficiency and P/T at 1173 keV obtained for different modes of data treatment. The statistical uncertainties are indicated in parenthesis. Tracking refers to default parameters (cf. Sec. 6.3). See text for details.

Input	Efficiency (%)	P/T (%)
AGATA (external trigger method)		
Core Common	2.38(2)	18.3(2)
Calorimetric	3.30(2)	32.2(3)
Tracked with single interactions	2.55(3)	37.5(4)
Tracked without single interactions	2.53(3)	42.3(5)
Add-back 100 mm	2.86(4)	24.6(2)
Geant4 simulations (external trigger method)		
Core Common	2.84(9)	22.5(6)
Calorimetric	4.21(8)	42.5(10)
Tracked with single interactions	2.53(8)	58.2(19)
AGATA only		
Sum-peak calorimetric	3.25(4)	30.0(5)

300 As seen in the table, the values derived for the absolute efficiency, ϵ , differ
 301 significantly for the various modes of extracting the energies from the AGATA
 302 detectors. In the conventional approach, the efficiency was determined only
 303 taking into account energy information from the central contact of each single
 304 crystal. This core-common treatment results in the lowest value of $\epsilon = 2.38(2)$ %
 305 and the poorest $P/T = 18.3(2)$ %. Since AGATA has no Compton-suppression
 306 shields, about 60 % of the Compton-scattered events escaping the crystals will
 307 increase the background of the spectra by producing counts in both neighbouring
 308 crystals. Therefore, such low value of the P/T is understood. A pronounced
 309 increase in both efficiency and P/T is observed when referring to AGATA as
 310 a calorimeter, namely $\epsilon = 3.30(2)$ % and $P/T = 32.2(3)$ %, respectively. The
 311 calorimetric mode takes into account not only full-absorption in a crystal, but
 312 also Compton-scattering into neighbouring crystals. Therefore, more events are
 313 registered in the full-energy peak, simply because energy portions, which the
 314 core-common mode predominantly interprets as background, are summed up.
 315 In general, the calorimetric mode is sensitive to summing up multiple γ rays,

316 particularly in case of high-fold cascading γ rays.

317 In order to apply tracking algorithms on the present data sets, an adjustment
318 in the data processing was implemented. The absolute efficiency measurement
319 relies on coincidences between AGATA and the reference EUROBALL capsule,
320 but only AGATA crystals are included in the tracking routine. Therefore, two
321 classes of detectors have been defined in the analysis procedure: one for the
322 EUROBALL capsule alone and the other one for all AGATA crystals, which
323 registered a signal in a coincident event. This allowed for a separate treatment
324 of different detectors taking part in coincident events, yet being implemented
325 in the same DAQ system. Finally, this approach led to an efficiency of $\epsilon =$
326 $2.55(3) \%$ and $P/T = 37.5(4) \%$. The efficiency is obviously lower than the one
327 in calorimetric mode of analysis, but P/T shows a significant improvement.

328 The results of the calorimetric mode suggest that summing up all energies
329 recorded by all crystals could enhance lower-energy contributions, leading to
330 somewhat deteriorated P/T . Additionally, this approach does not allow for
331 rejection of partially absorbed γ rays and, as stated in Sec. 3, around 40 % of
332 the detector surface is not covered by other neighbouring detectors. Therefore,
333 all partially absorbed γ rays are included in the calorimetric spectrum.

334 As compared to the calorimetric mode, the tracked mode results in better
335 P/T . Tracking relies on properly extracted sequences of γ -ray energies and
336 points and rejection of the γ rays that could not be reconstructed. Hence, it
337 replaces the Compton suppression shields to some extent. If performed success-
338 fully, it suffers less from background contributions.

339 As explained in Sec. 5.2, the single-interaction contributions, being clusters
340 with single hits in a detector, could be excluded from the spectrum obtained
341 after tracking. This modification yields an efficiency of $\epsilon = 2.53(3) \%$ and $P/T =$
342 $42.3(5) \%$. The single interactions are largely responsible for the low-energy part
343 of the spectrum, hence the better P/T values as seen in Tab. 1. Fig. 3 depicts
344 this property of the spectra obtained with and without single interactions. Due
345 to a hard-coded limit, the spectral response of single interactions extends up
346 to 800 keV. Recent work [36] suggests that those events account for $\sim 20 \%$ of

the photopeak yield at 1173 keV. Therefore, the efficiency value reported here might show a corresponding increase if setting the energy acceptance limit for the single interactions as high as the γ rays of ^{60}Co .

The sum-peak method (see Sec. 5.2.2) yields results similar to the calorimetric mode, namely $\epsilon = 3.25(4) \%$ and $P/T = 30.0(5) \%$.

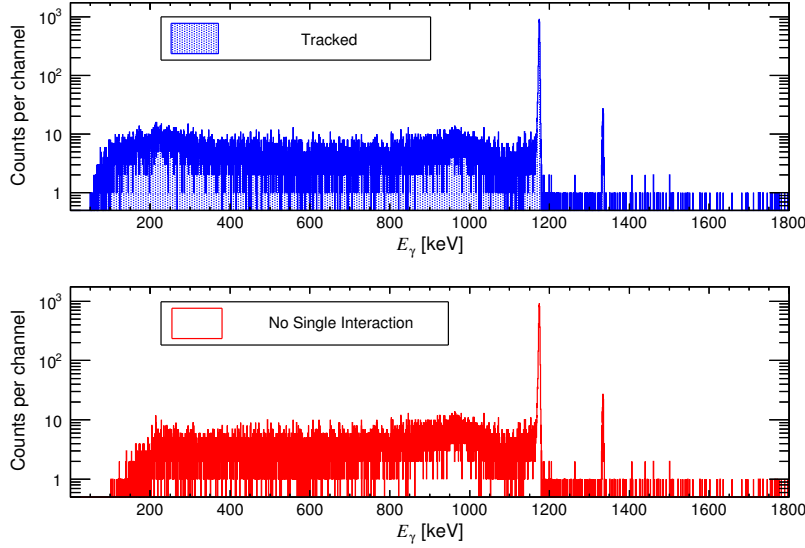


Figure 3: Spectra obtained with the MGT tracking algorithm [24] including (upper panel) and excluding single interaction points up to 800 keV (lower panel).

6.2. Normalized Efficiency

Different in-beam experiments performed with AGATA at GSI focused on different γ -ray energy regions. Therefore, a reliable reference in terms of an energy-dependent efficiency curve is needed. In this work, the energy extends up to ~ 3.3 MeV, i.e. one of the γ -ray transitions originating from the ^{56}Co source measurement. Three modes of operating AGATA at the data-analysis stage have been considered for the combined data set of ^{56}Co and ^{152}Eu : core common, calorimetric, and tracked with default parameter values (*Figure of Merit* FOM = 10, see Sec. 6.3). For the analysis of the three respective cases, two

spectra-analysis programs were used: tv [37] and TkT [38]. All γ -ray lines were least-squares fitted several times with a convolution of a Gaussian, a function that accounts for eventual tails on either right or left side of the centroid and another set of functions used to estimate the background. These fit results, including systematic uncertainties, were then sent to the code EFFIT, included in the Radware software package, which is using the parametrization detailed in [39] to extract the efficiency values from the measured peak intensities. The function used to fit the data points from the ^{56}Co and ^{152}Eu data sets is [39]:

$$\ln \epsilon(E_\gamma) = \{(A + B * x + C * x^2)^{-G} + (D + E * y + F * y^2)^{-G}\}^{-1/G} \quad (1)$$

with $x = \ln(E_\gamma/100)$, $y = \ln(E_\gamma/1000)$, E_γ in units of keV and A , B , C , D , E , F , G as fit parameters. Provided the absolute values of efficiency at 1173 keV (see Sec. 6.1 and Table 1), the aforementioned efficiencies can be readily normalized to the absolute efficiencies of the respective mode:

$$\epsilon_{\text{abs}}(E_\gamma) = N \cdot \epsilon(E_\gamma) \quad (2)$$

The efficiency curves according to Eq. 1 for different modes of analysis, alongside the experimental values for the calibration sources, are shown in Figs. 4, 5 and 7. The values of the fit and normalization parameters for all the curves are listed in Table 2.

Table 2: Fit parameters using the program EFFIT [39]. In all cases the parameters $C = 0$ and $G = 12$ were kept fixed. See text for details.

Dataset	Mode	Parameters					
		A	B	D	E	F	N
^{152}Eu and ^{56}Co	Core Common	8.42(19)	2.66(21)	6.410(3)	-0.573(6)	-0.071(6)	0.00454(3)
	Calorimetric	7.43(4)	1.69(5)	6.579(2)	-0.391(5)	—	0.00513(3)
	Tracked	6.80(5)	5.60(11)	6.3882(25)	-0.452(5)	—	0.00478(4)
^{152}Eu	Tracked FOM = 1.0	6.89(6)	5.73(12)	6.374(3)	-0.438(5)	—	0.00460(4)
	Tracked FOM = 0.1	7.7(3)	6.7(4)	6.274(4)	-0.421(6)	—	0.00440(5)
^{152}Eu	Add-back 100 mm	7.77(5)	1.86(6)	6.5653(24)	-0.413(5)	—	0.00423(5)
	Close Position	3.11(7)	2.9(3)	4.375(5)	-0.377(20)	-0.272(20)	0.038(2)

377 In case of the calorimetric spectrum, it is obvious that certain data points lie
 378 somewhat away from the least-squares fit (green stars in Fig. 4). Comparison
 379 of the γ -ray spectra has shown enhanced yields or slight modification in peak
 380 shapes. These differences in the shape of the peak in the calorimetric spectrum
 381 can arise from another process resulting in very similar energy deposition, i.e.
 382 summing of either two coincident γ rays or a γ ray and an X ray.

383 The drop in tracking efficiency below 100 keV is in part related to the ap-
 384 proximation made to compute effective distances in Ge. The approximation of
 385 a Ge sphere leads to an overestimation of the distance traveled by photons into
 386 the detector by up to a few mm. This overestimation is extremely penalizing
 387 for low-energy photons, which have very small ranges in Ge and are therefore
 awarded a poor figure of merit.

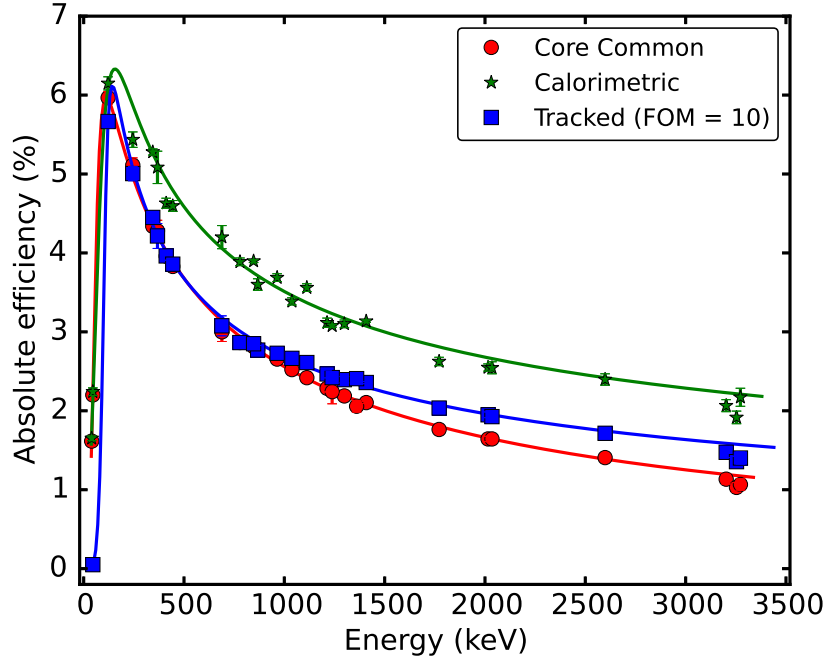


Figure 4: Efficiency curves obtained with spectra collected with ^{56}Co and ^{152}Eu normalized to the absolute efficiency determined at 1173 keV and confirmed by an external trigger method with the ^{152}Eu source data.

388 The results with the ^{152}Eu source at 'close position' (cf. Sec. 4) as well as the
 389 add-back treatment in case of the nominal position of the source are shown in
 390 Fig. 5. The two mentioned curves are compared to the core-common efficiency
 391 derived from the data collected with the same source at nominal position. In case
 392 of the core common at the close position the low-energy part of the spectrum is
 393 strongly affected by the lead shielding around the scattering chamber. Another
 394 cause of the attenuated yields is that this curve was derived by placing the ^{152}Eu
 395 source both in front and behind the plastic stopper. Consequently, in the first
 396 case the γ rays had to travel through the plastic medium, which reduced the low-
 397 energy contributions. In contrast to low energies, in the region of $E_\gamma \gtrsim 500$ keV
 398 the enhancement in the efficiency is ensured by the vicinity of the source.

399 6.3. Influence of the tracking algorithms

400 Two codes based on the forward-tracking algorithm mentioned in Sec. 2, both
 401 used by the AGATA community, have been employed to further investigate the
 402 effect of tracking on the performance. The details of the OFT performance are
 403 discussed in Ref. [36], whereas this work focuses on the MGT performance. The
 404 details of its implementation are, however, not subject of this work. They can
 405 be found in Ref. [24].

406 MGT and OFT tracking algorithms start by grouping certain interaction
 407 points which may be a part of the same physical event, resulting in one *track*.
 408 These groups of candidates are called *clusters*. The interaction points in each
 409 cluster are thus accepted in a given sequence or eventually rejected based on
 410 the conditions demanded by the algorithm.

411 In general, for the so-called FOM only one MGT parameter is varied, which
 412 defines how restrictive the algorithm is to the data sent as an input [24]. It
 413 quantifies divergence from the accepted χ^2 value, which is calculated between
 414 the ideal angle-energy sequence and the measured one. The higher the FOM
 415 value, the more data satisfy the MGT criteria, because the clusters are evaluated
 416 with greater 'tolerance', and vice versa. Consequently, for very high values of

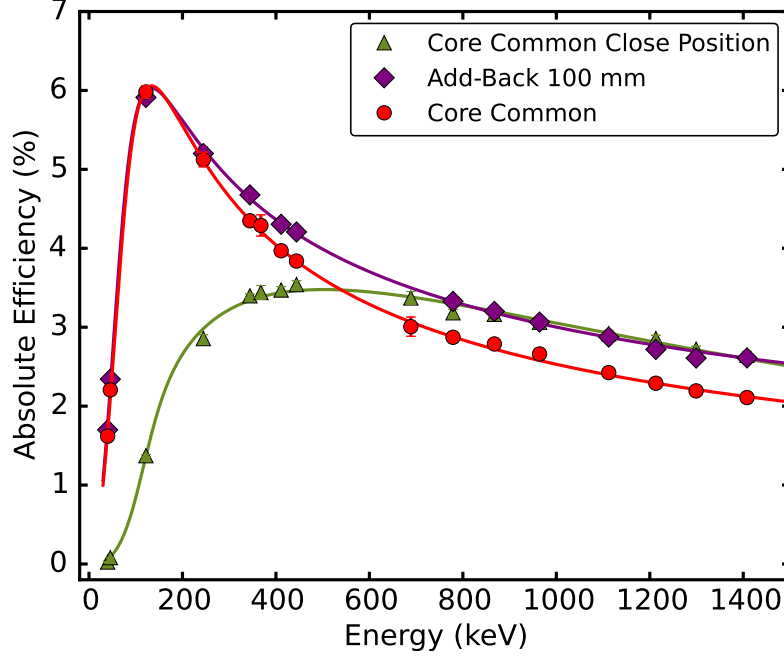


Figure 5: Efficiency curves obtained with spectra collected with ^{152}Eu normalized to the absolute efficiency determined at 1173 keV. The green curve (triangle up) and the red curve (circle) both represent the results when utilizing core common energy information but at two different positions: the green curve being closer to the array and the red at the nominal position. The purple curve (diamond) is obtained after adding back all hits in an event, which occurred within 100 mm radius from the reference point (highest energy release).

the FOM, more data has been interpreted as 'good'. But it also happens that the algorithm considers more events as background or it simply, due to the possible surplus of lower-energy contributions, does not classify the events in clusters well enough as a part of a real Compton scattering sequence.

The behaviour of tracking efficiency and P/T with respect to the absolute tracking efficiency has been tested in MGT [24] and OFT [25, 36], respectively. This was done by 'tuning' the FOM by changing the tracking parameters which are left free for the user to modify.

The effect of changing the FOM can be seen in Fig. 6. The curves show

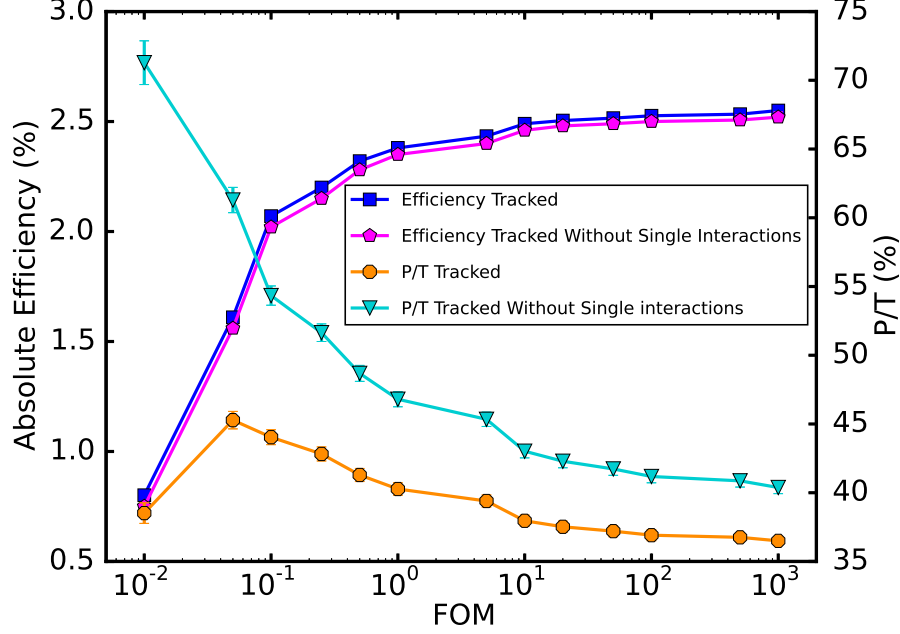


Figure 6: Influence of the FOM on the efficiency and P/T . FOM values range from 0.01 (left) to 1000 (right). All curves are obtained after applying the MGT tracking algorithm on ^{60}Co data. The blue curve (squares) represents the tracked efficiency trend for varying FOM. The magenta curve (pentagons) is a result of the same procedure, only without single interactions being treated. The orange curve (octagon) shows how the tracked P/T is affected by different values of the FOM. Similarly, the turquoise curve (triangle down) shows the behaviour of the same quantity, only referring to the tracked data without single interactions.

426 how the efficiency at 1173 keV and P/T change as the FOM varies. The ef-
 427 ficiency is increasing with higher FOM, unlike the P/T . For higher values of
 428 the FOM, more events have fulfilled the requirement of the algorithm. Hence,
 429 one can expect enhancement in the intensity of the full-energy peak, thus in
 430 the absolute efficiency. This increase comes about at the cost of deteriorated
 431 P/T . However, after subtracting single-interaction contributions in the tracked
 432 spectra (see Sec. 6.1), a significant enhancement in the P/T is obtained (see
 433 Fig. 6). In the range of the tested FOM values the absolute efficiency exhibits
 434 an increasing trend for the lower values of the FOM. This behaviour is less

pronounced for the rest of the range, as the absolute efficiency could not raise infinitely. Additionally, the further decrease of the P/T and the interplay of the two quantities suggest that the overall sensitivity of the system might not continue to improve significantly as the FOM increases. Therefore, the optimum value of the FOM should be decided by the user, in such a way to benefit from the changes in the values of the absolute efficiency and P/T . The MGT default value is set to $\text{FOM} = 10$ [24].

Moreover, consideration of the optimum FOM value is essential when applying tracking algorithms to different in-beam data sets. Beside Fig. 6, which shows that there is practically no increase in efficiency for $\text{FOM} \gtrsim 10$, there are several criteria to be considered. Firstly, how the value of the FOM might affect the results in an energy region of interest for a certain experiment. Secondly, if choosing the tracked spectrum with or without single interactions could serve as a reference alone, again depending on the energy region of interest. Finally, the selection of the best FOM might also depend on γ -ray multiplicity.

Additionally, the analysis of the ^{152}Eu data after tracking provides decisive input for treatment of the in-beam data. This implies the consideration of the ^{152}Eu dataset in the tracked mode alone, whilst varying the FOM. As in Section 6.2, the measured values of efficiency were normalized with respect to the absolute efficiency for different values of FOM and the fitting routine [39] generated the corresponding curves. Figure 7 shows that the general trend of the efficiency curve is independent of the variation in FOM. Instead, only the absolute value of efficiency is affected by changes of the FOM. As in case of ^{60}Co data, efficiency increases as the FOM increases. Following the analysis with different values of the FOM (see Fig. 6), the three values of the FOM were selected and displayed in Fig. 7, since further increase of the FOM does not affect the values of absolute efficiency significantly. This property is, as expected, in accordance with the analysis performed on the ^{60}Co data, which strengthens the argument of choosing the appropriate FOM value.

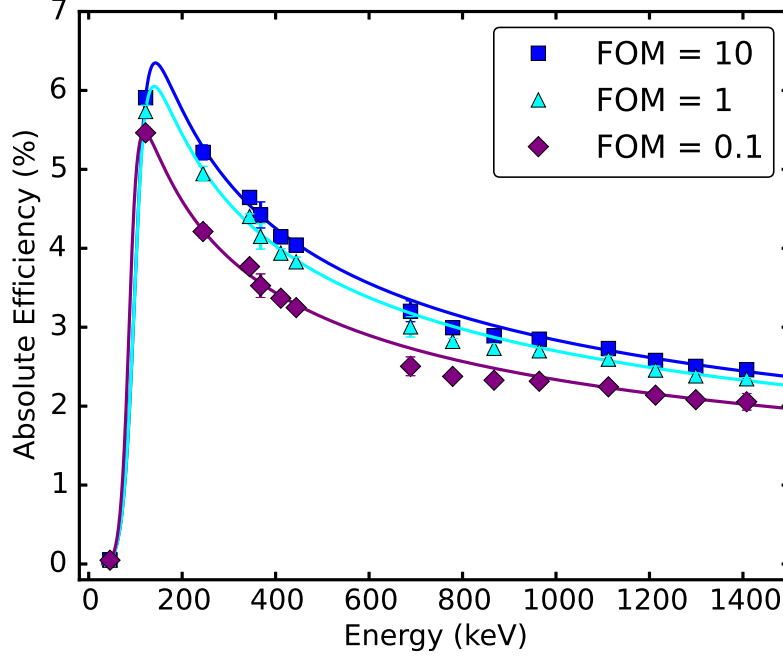


Figure 7: Efficiency curves obtained with a ^{152}Eu source by varying the FOM in the MGT tracking algorithm.

7. Geant4 Simulations

The developed Geant4 simulation comprises a realistic implementation of the set-up used during the source measurement including the scattering station with the holding ring structure as seen in Fig. 8. The evaluated results suggest the absolute efficiency for the core-common treatment of $\epsilon = 2.84(9) \%$ and $P/T = 22.5(6)\%$, $\epsilon = 4.21(8) \%$ and $P/T = 42.5(10) \%$ for operating AGATA in calorimetric mode and $\epsilon = 2.53(8) \%$ and $P/T = 58.2(19)\%$ for the tracking approach. The results from the simulation are somewhat higher than the experimental ones (see Table 1). They are also free from random coincidences. To first order, this can be associated to the difference between ideal detectors in the simulation and real detectors used for the experimental campaign at GSI. Despite these small discrepancies, detailed Geant4 simulations are a valuable

tool in optimizing the tracking parameters for (in-beam) data analysis.

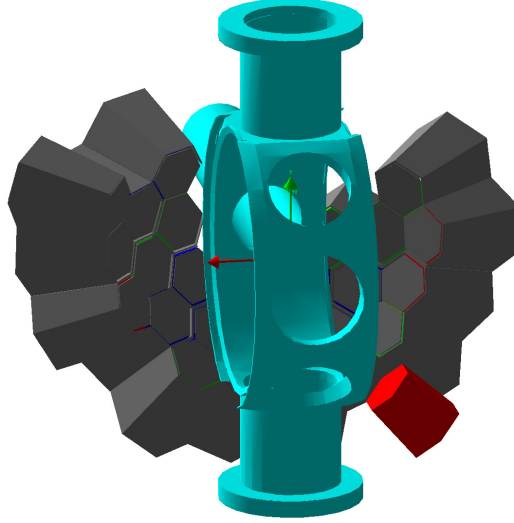


Figure 8: Geant4 visualization of the set-up. All AGATA crystals placed around the scattering chamber and the holding structure and the EUROBALL capsule are depicted solid. When used in the full PreSPEC-AGATA set-up, the beam enters from the front side. The EUROBALL capsule, shown in red, is located in the lower right corner.

476

477 8. Summary

478 The performance of the AGATA subarray at GSI has been presented, with
479 the main figures absolute efficiency and P/T being evaluated. Twenty one
480 AGATA crystals were employed in the experimental campaign at GSI, after
481 which the characterization measurements using calibration sources were per-
482 formed. Several practical aspects of applying the tracking algorithms on the
483 source data have been described, as well as some issues which need to be con-
484 sidered in case of in-beam data taken during the PreSPEC-AGATA campaign
485 at GSI. Additionally, the same data has been analyzed by exploiting only the

energy recorded by the central contact of all crystals, in the so-called core-common mode, as well as summing up energies recorded by all crystals, in the calorimetric mode. The measured values of the absolute efficiency do vary, but they do so in a predictable manner, as shown by the calorimetric efficiency being larger than the core-common. This consideration affects the in-beam data in such a way that the optimal treatment should be found for each experiment individually.

Moreover, further studies should focus on high γ multiplicity effects by both adding events recorded during measurements with sources and in in-beam events. This aspect should help understand the properties of γ -ray spectra taken in in-beam conditions.

Acknowledgements

This work has been supported by the European Community FP7-Capacities, contract ENSAR No. 262010 and by the Swedish Research Council and the Knut and Alice Wallenberg Foundation. This work has also been supported by the BMBF under Nos. 05P09RDFN4, 05P12RDFN8, by the LOEWE center HIC for FAIR, and by the UK Science and Facilities Research Council. AG and RMPV were partially supported by MINECO, Spain, under the grants FPA2011-29854-C04, FPA2014-57196-C5, Generalitat Valenciana, Spain, under the grant PROMETEOII/2014/019 and EU under the FEDER program.

Appendix A. Overview of Data Processing

All the operations on the data are performed with dedicated Narval [32] chains - the so-called actors on the data - implemented via C++ classes.

The data from the EUROBALL capsule was processed in the same way as from an AGATA crystal but with one exception, namely the *Tracking* actor. Furthermore, the EUROBALL capsule is a single non-segmented HPGe detector and the PSA was only formally performed on it. In practice, the algorithm

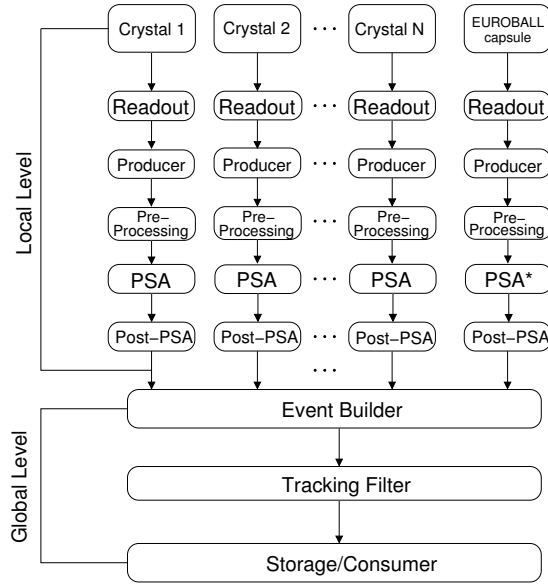


Figure A.1: Structure of AGATA Data Processing; here $N = 21$. Each box corresponds to a Narval actor. The EUROBALL capsule is also integrated in the system. The PSA associated to it was marked with an asterisk due to the fact that it was applied only formally. See text for details.

513 applied to it differs significantly from the sophisticated AGATA-tailored algo-
 514 rithms. Basically, every interaction is treated as if it had happened in the center
 515 of the crystal.

- [1] S. Akkoyun *et al.*, Nuclear Instruments and Methods in Physics Research Section A 668 (2012).
- [2] M.A. Delaplanque *et al.*, Nuclear Instruments and Methods in Physics Research Section A 430 (1999) 292.
- [3] N. Pietralla *et al.*, Eur. Phys. J. Web of Conferences 66 (2014) 02083.
- [4] P. Boutachkov *et al.*, to be published.
- [5] H. Geissel *et al.*, Nuclear Instruments and Methods in Physics Research Section B 70 (1992) 286.

- [6] S. Agostinelli *et al.*, Nuclear Instruments and Methods in Physics Research Section A 506 (2003) 250.
- [7] E. Farnea *et al.*, Nuclear Instruments and Methods in Physics Research Section A 621 (2010) 331.
- [8] C. Domingo-Pardo *et al.*, Nuclear Instruments and Methods in Physics Research Section A 694 (2012) 297.
- [9] C.W. Beausang and J. Simpson, Journal of Physics G: Nuclear and Particle Physics 22 (1996) 527.
- [10] J. Eberth and J. Simpson, Progress in Particle and Nuclear Physics 60 (2008) 283.
- [11] F.A. Beck, Proceedings of the Conference on Physics from Large γ -ray Detector Arrays, Berkeley, LBL 35687, CONF 940888, UC 413 (1994) 154.
- [12] J. Eberth, Progress in Particle and Nuclear Physics 28 (1992) 495.
- [13] J. Eberth *et al.*, Nuclear Instruments and Methods in Physics Research Section A 369 (1996) 139.
- [14] G. Duchêne *et al.*, Nuclear Instruments and Methods in Physics Research Section A 432 (1999) 90.
- [15] H.J. Wollersheim *et al.*, Nuclear Instruments and Methods in Physics Research Section A 573 (2005) 637.
- [16] J. Simpson *et al.*, Acta Physica Hungarica 11 (2000) 159.
- [17] D. Habs *et al.*, Progress in Particle and Nuclear Physics, 38 (1997) 1.
- [18] J. Gerl, Acta Physica Polonica B 34 (2003) 2481.
- [19] J. Simpson, Journal of Physics: Conference Series 41 (2006) 72.
- [20] A. Gadea *et al.*, Nuclear Instruments and Methods in Physics Research Section A 654 (2011) 654.

- [21] J. Van der Marel and B. Cederwall, Nuclear Instruments and Methods in Physics Research Section A 477 (2002) 391.
- [22] L. Milechina and B. Cederwall, Nuclear Instruments and Methods in Physics Research Section A 508 (2003) 394.
- [23] G.J. Schmid *et al.*, Nuclear Instruments and Methods in Physics Research Section A 430 (1999) 69.
- [24] D. Bazzacco, MGT code developed within the TMR program "Gamma-ray tracking detectors", Nuclear Physics A 746 (2004) 248c.
- [25] A.Lopez-Martens *et al.*, Nuclear Instruments and Methods in Physics Research Section A 533 (2004) 454.
- [26] A.M. Bruce *et al.*, to be published.
- [27] P. Golubev *et al.*, Nuclear Instruments and Methods in Physics Research Section A 723 (2013) 55.
- [28] I. Kojouharov, H.-J. Wollersheim, J. Gerl, M. Wolf, T. Engert. GSI Scientific Report 2008, GSI Report 2009-1 (2009) 235.
- [29] A. Georgiev *et al.*, IEEE Transactions on Nuclear Science 41 (1994) 1116.
- [30] N. Lalović *et al.*, Eur. Phys. J. Web of Conferences 93 (2015) 07007.
- [31] D. Ralet *et al.*, Nuclear Instruments and Methods in Physics Research Section A 786 (2015) 32.
- [32] X. Grave *et al.*, Real Time Conference 14th IEEE-NPSS (2005) 5.
- [33] R. Venturelli and D. Bazzacco, LNL Annual Report 2004, (2004) 220.
- [34] I. Kim, C. Park and H. Choi, Applied Radiation and Isotopes, 58 (2005) 199.
- [35] J. M. R. Hutchinson, W. B. Mann and P. A. Mullen, Nuclear Instruments and Methods 112 (1973) 187.

- [36] A.Lopez-Martens *et al.*, submitted to Nuclear Instruments and Methods in Physics Research Section A.
- [37] J. Theuerkauf, S. Esser, S. Krink, M. Luig, N. Nicolay, O. Stuch, and H. Wolters, program TV, University of Cologne, unpublished.
- [38] D. Bazzacco, The TkT spectrum viewer, private communication.
- [39] D.C. Radford, Nuclear Instruments and Methods in Physics Research Section A 361 (1995) 297.